Supporting Information

Tóth et al. 10.1073/pnas.1412449111

SI Materials and Methods

NUDT9 Expression and Purification. The cDNA for full-length mature human NUDT9 (residues 59–350) in the pJ411 vector was obtained from DNA2.0, included a C-terminal His_6-tag, and was codon-optimized (for *E. coli*). *E. coli* BL21 (DE3) strain was transfected with NUDT9-pJ411, grown at 37 °C in LB medium supplemented with 50 μg/mL kanamycin B sulfate, induced with 1 mM isopropyl-β-D-1-thiogalactopyranoside (IPTG), and further incubated for 3 h. Cells were harvested, resuspended in lysis buffer (20 mM Tris at pH 8.5, 100 mM NaCl) with added Halt Protease and Phosphatase Inhibitor Mixture (Thermo Scientific), and sonicated. The lysate was centrifuged (7,000 × *g*, 15 min, 4 °C) and the cleared supernatant was mixed with Ni-Sepharose 6 Fast Flow resin (GE Healthcare) for 3 h. The resin was then washed with 10 column volumes of lysis buffer, followed by 10 column volumes of lysis buffer containing 20 mM imidazole. The protein was eluted in a single step with lysis buffer containing 400 mM imidazole. The eluate was concentrated to ∼0.5 mL and loaded onto a Superdex 200 10/300 GL gel filtration column (GE Healthcare). Fractions containing monomeric NUDT9 were collected and dialyzed two times against 2 L of 20 mM Tris at pH 8.5. The final protein concentration was colorimetrically estimated to be ∼18 μM (∼0.6 mg/mL).

Enzymatic Assays and TLC. The enzymatic activity of NUDT9 was assessed in 20-μL reactions containing 1 μM purified NUDT9 and 20 mM nucleotide [ADPR, AMP, or AMPCPR; enzyme-to-substrate ratio, 1:20,000 (mol/mol)] in 50 mM Tris (pH, 8.5) supplemented with 16 mM $MgCl_2$. The reactions were incubated for 1 h at 37 °C. The respective controls did not contain NUDT9 and were treated identically. One-microliter aliquots from each reaction were placed on Polygram SIL G/UV_{254} plates (Macherey-Nagel) and developed in 200 mM NH_4HCO_3 in ethanol:water 7:3 (vol/vol). Nucleotides were visualized under UV light.

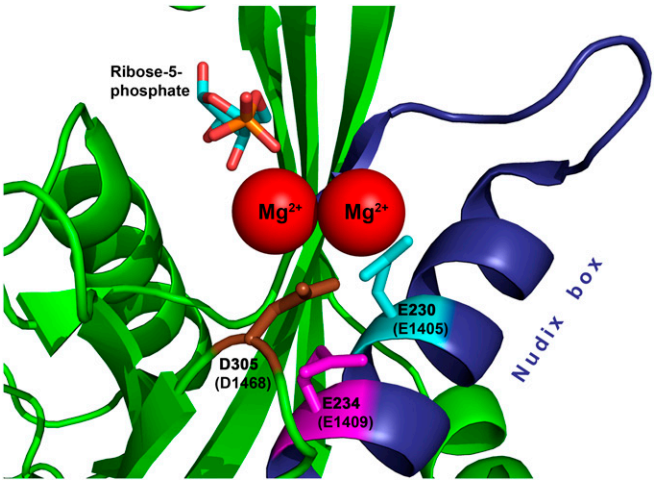

Fig. S1. Structure of the ligand-binding cleft in NUDT9. Ribbon diagram illustrating the ADPR binding cleft of human NUDT9 with bound ribose-5-phosphate, generated (PyMOL) from the coordinates of its crystal structure (PDB ID code 1QVJ). Residues discussed in the main text are highlighted. The Nudix motif is in dark blue. The ribose-5-phosphate (in sticks) is coordinated by Mg^{2+} ions (red spheres), stabilized by residue E230 (cyan; this residue aligns with I1405 in the NUDT9-H domain of TRPM2). Substitution of conserved residue E234 (magenta), corresponding to E1409 in NUDT9-H, destroys the enzymatic activity of NUDT9. Residue D305 (brown), downstream of the Nudix motif, aligns with the proposed catalytic base of *E. coli* ADPRase; the functionally equivalent residue in TRPM2 is D1468.

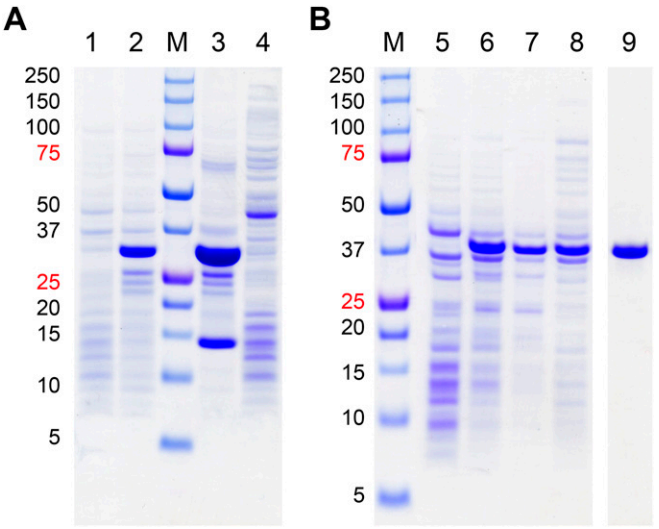

Fig. S2. Expression and solubility of NUDT9-H and NUDT9. Coomassie-stained SDS/PAGE images showing the expression and solubility of (*A*) NUDT9-H and (*B*) NUDT9. Total cell pellets of noninduced (lanes 1 and 5) and induced (lanes 2 and 6) *E. coli* BL21 (DE3) show the overexpressed protein. On sonication, NUDT9-H is found predominantly in the pellet fraction (lane 3) and not in the supernatant (lane 4), whereas NUDT9 is only partially lost in the pellet (lane 7) and is also abundantly present in the supernatant (lane 8). After solubilization of the NUDT9-H inclusion bodies using 7 M urea or 6 M guanidine/HCl, the protein reprecipitated on dilution of the chaotropic agent. Lane 9 shows NUDT9 purified from the supernatant by Ni-affinity chromatography, followed by gel filtration. Numbers on the left of the gel images identify the sizes (in kDa) of the size marker ladder (*Precision*, Bio-Rad) bands (lanes M).

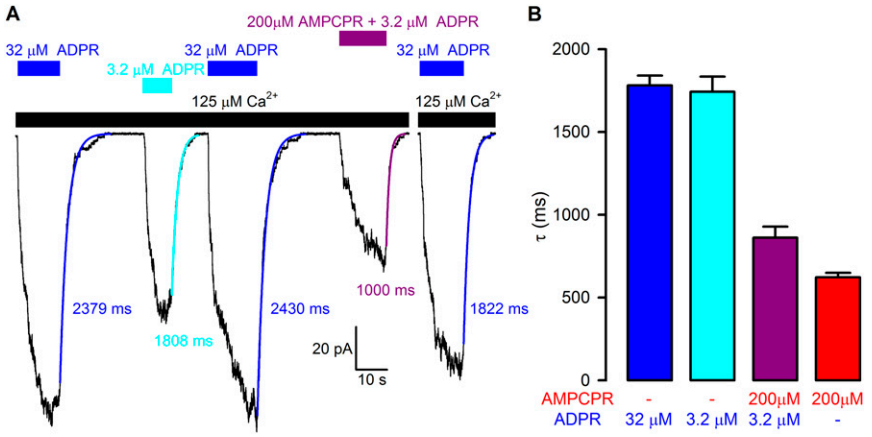

Fig. S3. Mixtures of ADPR and AMPCPR do not arrest TRPM2 channels in the bursting state. (*A*) Decay time courses on nucleotide removal of macroscopic T5L-TRPM2 currents activated in the presence of saturating Ca^{2+} by brief applications of saturating (32 μM) ADPR (blue bars), 3.2 μM ADPR (cyan bar), or a mixture of 200 μM AMPCPR plus 3.2 μM ADPR (purple bar); for both nucleotides, the latter concentrations are ~3 × $K_{1/2}$ (cf. Fig. 3C). Colored lines are single-exponential fits, with time constants indicated. (*B*) Mean ± SEM deactivation time constants of T5L-TRPM2 channels opened by 32 μM ADPR (blue, replotted from Fig. 4C), 3.2 μM ADPR (cyan), 3.2 μM ADPR + 200 μM AMPCPR (purple), or 200 μM AMPCPR (red, replotted from Fig. 4C), from experiments such as the ones shown in *A*.

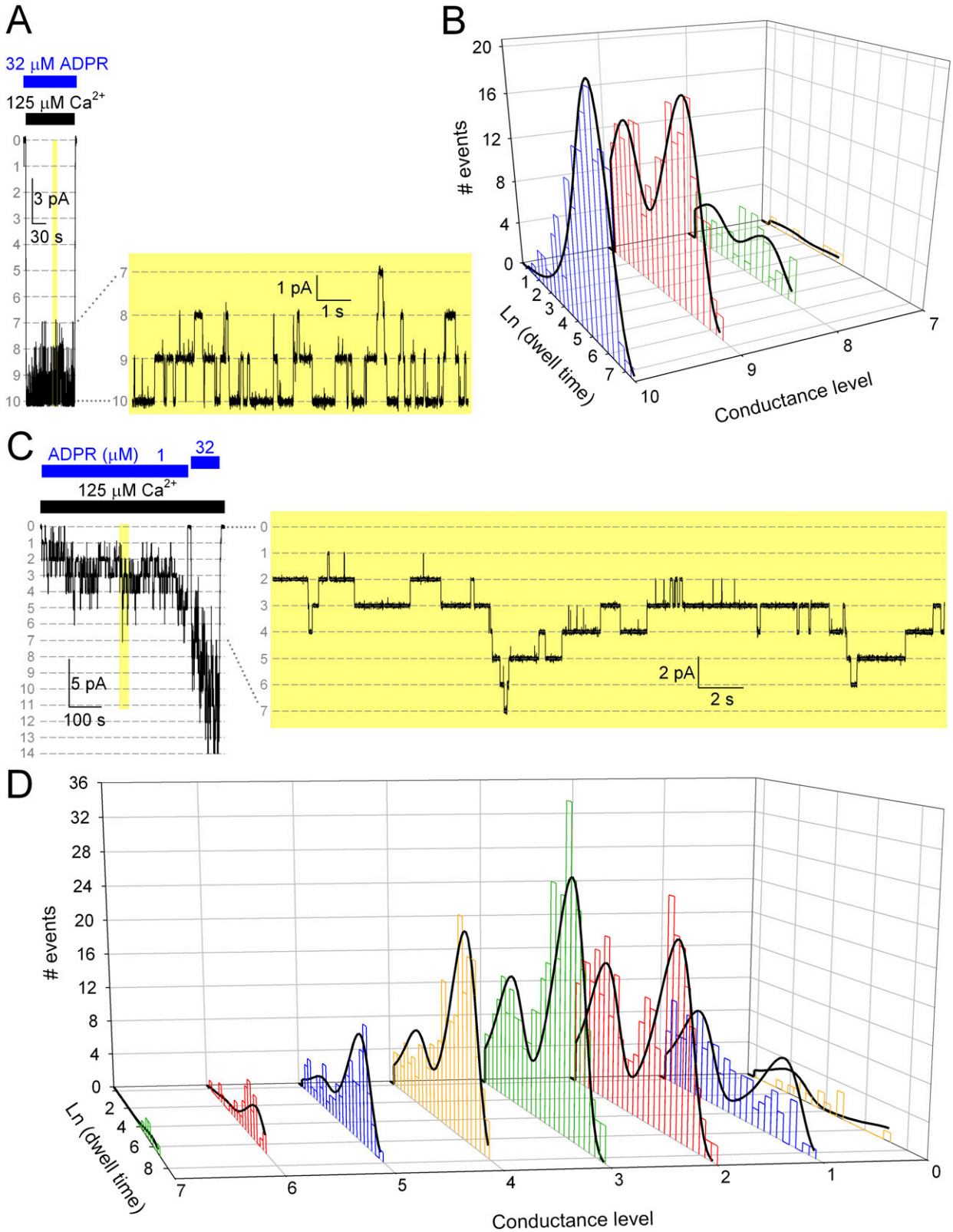

Fig. S4. Kinetic analysis of multichannel patches by simultaneous maximum likelihood fitting to the dwell-time histograms of all conductance levels. (*A* and *C*) Individual channel gating transitions remain well resolvable in patches containing multiple active TRPM2 channels. Steady-state channel currents from patches containing (*A*) 10 and (*C*) 14 active T5L TRPM2 channels in the presence of 125 μM Ca^{2+} and (*A*) 32 or (*C*) 1 μM ADPR; channel number was estimated in each patch from high-P_o segments in the presence of 32 μM ADPR as the maximum number of simultaneously open channels. Yellow boxes highlight segments of record shown to the right at an expanded time scale; note that gating transitions are well resolved. Bandwidth, 200 Hz; trace in *A* replotted from ref. 1. (*B* and *D*) Logarithmically binned dwell-time histograms (colored bar charts) of steady-state current segments in 125 μM Ca^{2+} and (*B*) 32 or (*D*) 1 μM ADPR plotted

Legend continued on following page

individually for each conductance level (cf. gray dashed lines in *A* and *C*), obtained from the traces in *A* and *C*, respectively, by half-amplitude threshold crossing analysis, using an imposed fixed dead time of 0.9 ms. The histogram set in *B* contains 472 events, and that in *D* 1190 events, in total. Families of solid black curves illustrate the simultaneous maximum likelihood fits of the sets of dwell-time histograms by the $C_{s(1)}$-$O_{(3)}$-$C_{f(2)}$ scheme, accounting for the fixed dead time (2), with the four rate constants r_{13}, r_{31}, r_{32}, and r_{23} as free parameters. Fitted rate constants were (*B*) $r_{13} = 6.6\ s^{-1}$, $r_{31} = 0.23\ s^{-1}$, $r_{13} = 0.24\ s^{-1}$, and $r_{13} = 385\ s^{-1}$, and (*D*) $r_{13} = 0.046\ s^{-1}$, $r_{31} = 0.17\ s^{-1}$, $r_{13} = 0.33\ s^{-1}$, and $r_{13} = 135\ s^{-1}$. Calculated bursting parameters (cf. Fig. 6 *B*–*F*) were (*B*) $\tau_b = 4{,}415$ ms, $\tau_{ib} = 150$ ms, $\tau_o = 2{,}145$ ms, $\tau_f = 2.6$ ms, and $n_f = 1.1$, and (*D*) $\tau_b = 5{,}082$ ms, $\tau_{ib} = 21{,}874$ ms, $\tau_o = 1{,}988$ ms, $\tau_f = 7.4$ ms, and $n_f = 1.9$.

1. Tóth B, Csanády L (2012) Pore collapse underlies irreversible inactivation of TRPM2 cation channel currents. *Proc Natl Acad Sci USA* 109(33):13440–13445.
2. Csanády L (2000) Rapid kinetic analysis of multichannel records by a simultaneous fit to all dwell-time histograms. *Biophys J* 78(2):785–799.

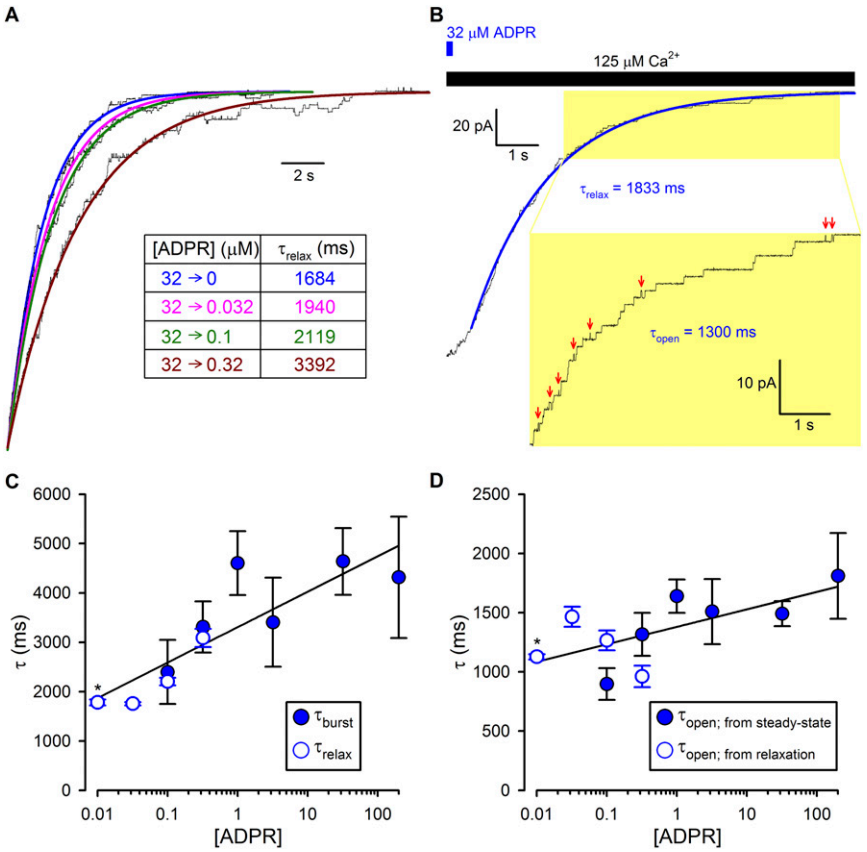

Fig. S5. Slight dependence of mean open times and mean burst durations on ADPR concentration. (*A*) Decay time courses of macroscopic T5L-TRPM2 currents on sudden lowering of activating ADPR from 32 μM to 0, 0.032, 0.1, or 0.32 μM. Colored lines are single-exponential fits with time constants indicated in the adjacent table. (*B*) Decay time course of macroscopic T5L-TRPM2 current on sudden ADPR removal and single-exponential fit (blue line). Mean open times (τ_{open}) at zero nucleotide concentrations were calculated from the final segments of such macroscopic current relaxations after nucleotide removal, in which individual channel transitions could be clearly resolved (yellow box). Such stretches were idealized by half-amplitude threshold crossing, and τ_{open} was obtained as the cumulative open time divided by the total number of closing transitions. The segment in the yellow box is expanded in the inset and illustrates two types of closures: irreversible staircase-like closures, from which the channels do not reopen, and flickery closures (red arrows), from which the channels reopen even in the absence of bath nucleotide. Note that τ_{open}, calculated by taking into account both types of closures, is shorter than the relaxation time constant. (*C* and *D*) Comparison of single-channel steady-state (*C*) τ_{burst} and (*D*) τ_{open} (closed symbols, replotted from Fig. 6 *B* and *D*) with (*C*) the relaxation time constants and (*D*) the calculated mean open times after sudden lowering of the concentration of ADPR from 32 μM to a submicromolar concentration (open symbols). Leftmost open symbols (denoted by asterisk) depict parameters measured for complete removal of ADPR. Solid straight lines are tentative linear regressions through the data and confirm significant positive trends ($r = 0.86$ and 0.67, respectively).